Subterahertz chaos generation by means of nonlinear effects of a linear resonator

A.E. Hramov[1,4], V. Makarov[1], A.A Koronovskii[1,4], S.A. Kurkin[1], M.B. Gaifullin[2], N.V. Alexeeva[2], K.N. Alekseev[2], M.T. Greenaway[3], T.M. Fromhold[3], A. Patanè[3], F.V. Kusmartsev[2], V.A. Maksimenko[4], O.I. Moskalenko[4] and A.G. Balanov[2,1]

[1] *Faculty of Nonlinear Processes, Saratov State University, Astrakhanskaya 83, Saratov, 410012, Russia*

[2] *Department of Physics, Loughborough University, Loughborough LE11 3TU, United Kingdom*

[3] *School of Physics and Astronomy, University of Nottingham, Nottingham NG7 2RD, United Kingdom*

[4] *Saratov State Technical University, Politechnicheskaja 77, Saratov, 410054, Russia*

(ΩDated: November 22, 2013)

We investigate the effects of a linear resonator on the high-frequency dynamics of electrons in electronic devices exhibiting negative differential conductance. We show that the resonator strongly affects both the DC and AC transport characteristics of the device, inducing quiasiperiodic and high-frequency chaotic current oscillations. The theoretical findings are confirmed by experimental measurements of a GaAs/AlAs miniband semiconductor superlattice coupled to a linear microstripe resonator. Our results are applicable to other active solid state devices and provide a generic approach for developing modern chaos-based high-frequency technologies including broadband chaotic wireless communication and for super-fast random-number generation.

PACS numbers: 05.45.-a, 73.21.-b, 72.20.Ht
Keywords:

The interaction of matter with electromagnetic (EM) waves confined within a resonator remains one of the most important and widespread problems in physics. This generic system has many implications in different areas of science including cold atoms [1], quantum engineering [2], metamaterials [3], THz and nanoscale lasers with sub-millimeter wavelength cavities [4, 5]. In electronics and optics, resonators are often used to enhance the generated power [4] or to tune the frequency of radiated EM waves [6]. The action of a high quality resonator may also provide a way to achieve monochromatization and coherence purification of electromagnetic output [7].

Devices that exhibit negative differential conductance (NDC) have great potential to operate in the technologically important GHz-THz frequency range, even at room temperature. If the product of the carrier concentration within the device and the sample length exceeds a critical value [8], the NDC triggers the formation of propagating charge domains [9], and associated active EM properties. This includes an ability to amplify an injected high frequency signal [10]. In our study, we focus on a semiconductor superlattice (SL), where the physical mechanism for NDC is the onset of fast (typically THz) Bloch oscillations in a single miniband [11–13]. Recently, it was shown that both the number and the dynamics of the domains can be effectively controlled by applying alternating electric or tilted magnetic fields [14–16]. The propagating, and periodically pulsing, charge domains in miniband GaAs/AlGaAs SLs produce a powerful high-frequency (hundreds of GHz) radiation [17] and very effective frequency multiplication up to several THz [18]. However, the influence of EM resonators on the electron dynamics in SLs is still largely unexplored [19].

To address this question we theoretically and experimentally study how the eigenfrequency and the quality factor of a linear resonator affect the collective electron dynamics and resulting high-frequency current oscillations in a SL. It is already known that due to nonlinearities the semiconductor heterostructures can generate chaos (see, e.g., [12, 20]). However, here we show, counter-intuitively, that even a *linear* resonator can drive regular oscillations chaotic when the oscillations originate from the NDC. By changing the voltage applied to the coupled SL and resonator one can switch between periodic, quasiperiodic and chaotic current oscillations in SLs that exhibit *only periodic* oscillations in the absence of a resonator. Our theoretical analysis and experiments are in good quantitative agreement. The phenomena that we identify suggest applications for new resonant control of dynamics in solid state systems with NDC.

Note, the high-frequency chaotic generators are currently on strong demand in number of modern key technologies including fast random-number generation (see [21] and references therein) and chaos-based communication systems [22–24]. However, in contrast to optical frequency range, the chaotic sub- and terahertz generators are still underdeveloped [21]. Our findings propose a generic approach and physical effects which can be used for a development of such generators.

We consider a SL interacting with a resonator, as shown schematically in Fig. 1(a). We assume that only one EM field mode is excited in the resonator. This mode is characterized by the eigenfrequency, f_Q, and quality factor, Q. In this case the resonator can be represented by the equivalent RLC-circuit shown in Fig. 1(b) and described by the non-stationary Kirchhoff equations. The SL serves as a generator of electric current, I, controlled by a voltage, $V_{sl}(t)$, dropped across SL, which includes both the DC supply voltage, V_0, and the AC voltage, $V_1(t)$, generated by the RLC-circuit.

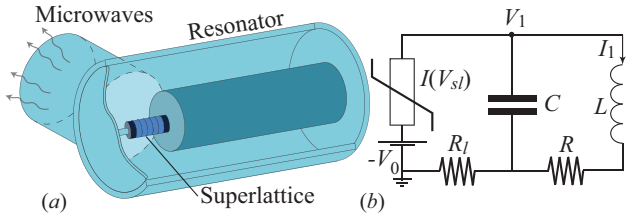

FIG. 1: (Color online) (a) Schematic diagram of a semiconductor superlattice coupled to an external EM resonator. (b) Equivalent circuit for a SL interacting with an external single-mode resonator. Here C, L and R are the equivalent capacitance, inductance and resistance of the resonator, $I(V_{sl})$ is the current through the SL, with voltage V_{sl} dropped across it, and V_0 is the DC supply voltage. The load resistance is $R_l = 0.1\,\Omega$.

To calculate the charge dynamics in the SL, and thus obtain the current-voltage, $I(V_{sl})$, characteristics, we numerically solve the discrete current continuity and Poisson equations. To make our model realistic we follow the approach described in [16], with SL parameters taken from recent experiments [14, 15]. The miniband transport region is discretized into $N = 480$ layers, each of width $\delta x = 0.24\,\text{nm}$, small enough to approximate a continuum and ensure convergence of the numerical scheme. The discretized current continuity equation is

$$e\delta x \frac{dn_m}{dt} = J_{m-1} - J_m, \qquad m = 1 \ldots N, \tag{1}$$

where $e > 0$ is the electron charge magnitude, n_m is the charge density at the right-hand edge of m^{th} layer, at position $x = m\delta x$, and J_{m-1} and J_m are the areal current densities at the left and right hand boundaries of the m^{th} layer within a drift-diffusion model

$$J_m = e n_m v_d\left(\overline{F}_m\right), \tag{2}$$

where $\overline{F}_m$ is the mean field in the m^{th} layer [16]. The drift velocity, $v_d(\overline{F})$, corresponding to electric field, $\overline{F}$, can be calculated as in [25]:

$$v_d = \frac{\Delta d}{2\hbar}\frac{I_1(\Delta/2k_BT)}{I_0(\Delta/2k_BT)}\frac{e\overline{F}d\tau/\hbar}{1+(e\overline{F}d\tau/\hbar)^2}, \tag{3}$$

where $d = 8.3$ nm is the period of the SL, $\Delta = 19.1\,\text{meV}$ is the miniband width, $T = 4.2\,\text{K}$ is the temperature, k_B is the Boltzmann constant and $I_n(x)$, where $n = 0, 1$, is a modified Bessel function of the first kind.

The electric fields F_m and F_{m+1} at the left- and right-hand edges of the m^{th} layer respectively, are related by the discretized Poisson equation

$$F_{m+1} = \frac{e\delta x}{\varepsilon_0\varepsilon_r}\left(n_m - n_D\right) + F_m, \quad m = 1 \ldots N, \tag{4}$$

where ε_0 and $\varepsilon_r = 12.5$ are, respectively, the absolute and relative permittivities and $n_D = 3\times10^{22}\ \text{m}^{-3}$ is the n-type doping density in the SL layers [14]. We assume that the emitter and collector contacts are ohmic and that the field in the contacts is given by F_0. In this case, the current density injected into the contact layers of the SL is $J_0 = \sigma F_0$, where $\sigma = 3788\ \text{Sm}^{-1}$ is the conductivity of the heavily-doped emitter [16]. The voltage, V_{sl}, dropped across the SL defines a global constraint:

$$V_{sl} = U + \frac{\delta x}{2}\sum_{m=1}^{N}(F_m + F_{m+1}), \tag{5}$$

where the voltage, U, dropped across the contacts includes the effect of charge accumulation and depletion in the emitter and collector regions, and the voltage across the contact resistance, $R = 17\ \Omega$ [16]. The current through the device can be defined as

$$I(t) = \frac{A}{N+1}\sum_{m=0}^{N} J_m, \tag{6}$$

where $A = 5\times10^{-10}\ \text{m}^2$ is the cross-sectional area of the SL [12, 14, 16].

We apply Kirchoff's equations to the equivalent circuit shown in Fig. 1(b) and obtain the following equations

$$\frac{dV_1}{dt} = \frac{I(V_{sl}) - I_1}{C}, \quad \frac{dI_1}{dt} = \frac{V_0 - V_{sl} + RI_1 + R_lI(V_{sl})}{L}, \tag{7}$$

where $V_1(t)$ and $I_1(t)$ are, respectively, the voltage across the capacitor and the current through the inductor [see Fig. 1(b)]. Thus, the voltage dropped across the SL is $V_{sl} = V_1 + V_0$. The eigenfrequency of the resonator is $f_Q = 1/(2\pi\sqrt{LC})$ and the quality factor is $Q = (1/R)\sqrt{L/C}$.

The current through the SL is either constant or oscillates depending on the voltage, V_0, applied to the circuit. If the SL is decoupled from the resonator ($V_1 = 0$), its current-voltage characteristic, $I(V_{sl})$, is of the Esaki-Tsu type [11] and the current oscillations are *always* periodic [16]. However, if the resonator is coupled to the SL, the circuit behavior changes greatly.

In the coupled regime, the $I(V_{sl})$–characteristic obtained by averaging the current $I(t)$ [Eq. 6] over time is shown in Fig. 2 by the dark grey (red online) curve. This curve has a similar form to the Esaki-Tsu curve [11]. For low voltages, it is ohmic and the current attains a maximum value when $V_0 = V_{crit}$ (marked by the arrow in Fig. 2). Thereafter, the current tends to decrease with increasing V_0 due to the onset of Bloch oscillations. However, for $V_0 > V_{crit}$ there is a series of peaks in $I(V_0)$, which do not occur in the absence of the resonator. These peaks correspond to the transitions between different periodic and chaotic dynamical regimes. To illustrate this, in Fig. 2 we superimpose a bifurcation diagram in which each point shows the local maximum value of $V_1(t)$ (RH scale) obtained for each V_0 value (omitting any initial transient behavior). Thus, for

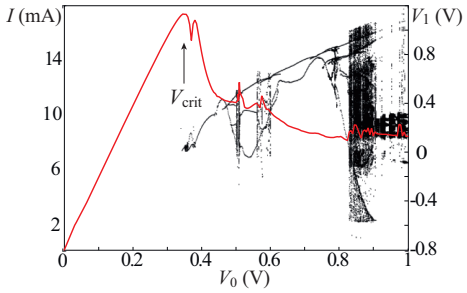

FIG. 2: (Color online) $I(V_0)$ (red curve, scale on LH axis) calculated for a SL coupled to a resonator with $f_Q = 13.81\,\mathrm{GHz}$ and $Q = 150$. Overlaid is the bifurcation diagram (black dots) of the voltage oscillations, $V_1(t)$, (RH axis) versus V_0. The critical value $V = V_{crit}$ for the onset of calculated microwave generation is shown by the arrow.

a given V_0, a single point in the bifurcation diagram represents either a steady state or periodic $V_1(t)$ oscillations. Similarly, several separated points indicate period-added oscillations and a complex set of points implies either quasiperiodic or chaotic behavior. Fig. 2 reveals that each peak in the $I(V_0)$ curve corresponds to a transition between different types of dynamics in the bifurcation diagram. With increasing V_0, the dynamics changes first from a steady state solution to periodic oscillations when $V_0 \approx V_{crit}$. Thereafter, increasing V_0 induces multiple transitions between periodic and aperiodic oscillations, with each transition corresponding to a peak in the $I(V_0)$ curve. For example, when $V_0 \approx 0.5\,\mathrm{V}$ and $V_0 \approx 0.83\,\mathrm{V}$, we find peaks in the $I(V_0)$ curve and a transition between periodic and chaotic dynamics. The presence of chaos is confirmed by calculation of the Lyapunov exponents [26] (see Fig. S1 in Supplemental Material [27]). Note, the SL demonstrates a transition to chaos through intermittency with increase of the DC voltage, V_0 (see Supplemental Material [27], Fig. S2).

Transitions between different oscillatory regimes can also be realized by fixing the parameters of the SL and varying those of the resonator. For example, Fig. 3(a) shows the bifurcation diagram obtained by varying the resonator eigenfrequency, f_Q, when $V_0 = 0.54\,\mathrm{V}$. The variation of f_Q produces a number of bifurcations leading to the appearance and disappearance of aperiodic oscillations (represented by a complex set of points). In particular, we find that the regions of chaotic oscillations [shaded grey in Fig. 3(a)] are separated by a narrow region of periodic oscillations.

To gain further insight into the transitions between the dynamical regimes, in Fig. 3(b,c) we show the Fourier power spectra of the $V_1(t)$ oscillations for f_Q values $f_{Qp} = 13.07\,\mathrm{GHz}$ (b) and $f_{Qc} = 13.81\,\mathrm{GHz}$ (c) [marked by vertical red dashed lines in Fig. 3(a)] before and after the onset of chaos at $f_Q = 13.6\,\mathrm{GHz}$ [upper arrow in Fig. 3(a)]. Figures 3(d) and (e) show the corresponding phase portraits of the oscillations $[V_1(t), V_1(t-\tau)]$ con-

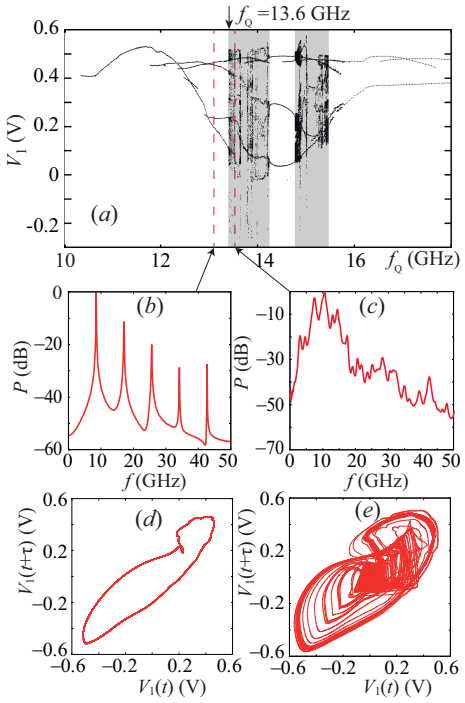

FIG. 3: (Color online)(a) Bifurcation diagram showing local maxima, V_1, of the voltage oscillations, $V_1(t)$, versus f_Q at $V_0 = 0.54\,\mathrm{V}$. The grey panels mark the f_Q ranges where chaotic oscillations occur. (b,c) Power spectra of voltage oscillations, $V_1(t)$, for the resonator frequencies [vertical red dashed lines in (a)] $f_{Qp} = 13.07\,\mathrm{GHz}$ (b) and $f_{Qc} = 13.81\,\mathrm{GHz}$ (c). The corresponding time-delayed phase trajectories are shown in (d) and (e).

structed by the Takens method (the method of delayed coordinates) [28] with time delay $\tau = 0.3\,\mathrm{ps}$. Before the transition, when $f_{Qp} = 13.07\,\mathrm{GHz}$, the oscillations have a discrete spectrum [Fig. 3(b)] with equidistant peaks reflecting the periodic character of $V_1(t)$, which is confirmed by the closed phase trajectory [Fig. 3(d)]. After the transition, when $f_{Qc} = 13.81\,\mathrm{GHz}$, the frequency spectrum becomes continuous [Fig. 3(c)], and the trajectory in Fig. 3(e) fills the phase space, indicating chaotic dynamics. We emphasise that the appearance of chaos in a SL coupled to a *linear* resonator is surprising because chaos is a fundamentally *nonlinear* phenomenon. In addition, the SL does not reveal chaotic behavior when it is decoupled from the resonator.

In Fig. 4 we show the parameter space (f_Q, Q), illustrating the regions of chaotic dynamics [shaded grey]. The figure reveals that chaos is a robust phenomenon, which appears for a wide range of f_Q values. However, the figure also reveals that the onset of chaos depends critically on the Q-factor of the resonator. Chaotic oscillations only appear when Q exceeds a threshold value, which, for $V_0 = 0.54\mathrm{V}$, is ≈ 50. Increasing Q above 50, the width of the chaotic region in f_Q initially increases and then saturates for $Q > 150$. Since the fre-

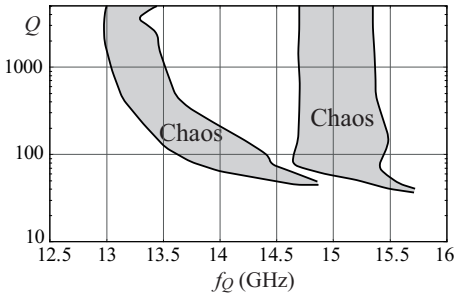

FIG. 4: Parameter plane (f_Q, Q) showing where the $I(t)$ and $V_1(t)$ oscillations are chaotic (grey) or periodic (white) when $V_0 = 0.54\,\mathrm{V}$.

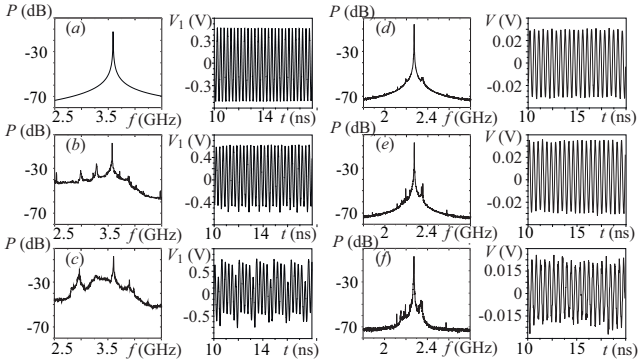

FIG. 5: The numerically $(a$-$c)$ and experimentally $(d$-$f)$ obtained power spectra (left panels) and $V_1(t)$ oscillations (right panels) for the SL coupled to two resonators with V_0 = (a) 0.42 V, (b) 0.43 V, (c) 0.44 V; (d) 0.34 V, (e) 0.35 V, (f) 0.355 V.

quency of the current oscillations in the decoupled SL is $f_{SL} = 16.76\,\mathrm{GHz}$ when $V_0 = 0.54$ V, we conclude that chaos occurs when f_Q is well detuned from f_{SL}.

In addition to the effects of a coupled resonator, it is also important to consider how any parasitic capacitance and inductance associated with the wires and contacts of the SL device affect the current oscillations. To study this we consider an equivalent circuit, which takes into account this parasitic reactance in addition to the influence of an external resonator (see [27], Fig. S3 for an equivalent circuit of a SL coupled to two resonators). Our calculations reveal that this system can also exhibit chaotic oscillations. This is shown in Fig. 5$(a$–$c)$ where a transition from periodic (a) to quasiperiodic (b,c) current oscillations occurs with increasing V_0. Here, the parasitic resonator is characterized by the quality factor $Q_1 = 20$ and eigenfrequency $f_{Q1} = 2.82\,\mathrm{GHz}$ and the external resonator has parameters $Q_2 = 37.6$ and $f_{Q2} = 3.1\,\mathrm{GHz}$.

When $V_0 = 0.42$ V [Fig. 5(a)] the system exhibits periodic $V_1(t)$ oscillations (right panel) with a single dominant frequency $\approx 3.5\,\mathrm{GHz}$ in the Fourier power spectrum (left panel). Increasing V_0 to 0.43 V [Fig. 5(b)] changes the character of the oscillations: the Fourier spectrum starts to show peaks at combination frequencies (left panel), and the $V_1(t)$ oscillations become quasiperiodic (right panel). Finally, by increasing V_0 to 0.44 V [Fig. 5(c)] we find that the $V_1(t)$ oscillations (right panel) are chaotic with a broad spectrum (left panel). This evolution of the $V_1(t)$ curves and Fourier spectra suggests that chaos appears via the breakdown of quasiperiodicity [29].

To verify our theoretical predictions, we performed experimental measurements on a SL with parameters corresponding to those of our model. The SL was grown by molecular beam epitaxy on a (100)-oriented n-doped GaAs substrate. It comprises 15 unit cells, which are separated from two heavily n-doped GaAs contacts by Si-doped GaAs layers of width 50 nm and doping density $1 \times 10^{23}\ \mathrm{m}^{-3}$. Each unit cell, of width d and Si doped at $3 \times 10^{22}\ \mathrm{m}^{-3}$, is formed by a 1 nm thick AlAs barrier and a 7 nm wide GaAs quantum well (QW) with 0.8 InAs monolayers at the center of each QW. The InAs layer facilitates the direct injection of electrons into the lowest energy miniband and also creates a large enough minigap to prevent interminiband tunneling [30]. For electrical measurements, the SL was processed into circular mesa structures of diameter 20 μm with ohmic contacts to the substrate and top cap layer.

The SL was connected to an external high-frequency strip line resonator with a resonant frequency $f_{Q2} = 2.38\,\mathrm{GHz}$ (see [27], Fig. S4, S5). Electrodynamic simulations of the SL sample and our direct measurements showed that the contact bonding acts like the parasitic resonator discussed above, with a resonant frequency of $f_{Q1} = 0.87\,\mathrm{GHz}$. A LeCroy SDA 18000 serial data analyzer was used to measure the voltage oscillations generated by the SL.

Without the external resonator (when only the parasitic resonator is present), our measurements reveal periodic $V_1(t)$ oscillations with a frequency close to the resonant frequency of the parasitic resonator [15]. However, when the external resonator is connected, the results reveal a transition to chaos, which agrees qualitatively well with our theoretical predictions, see Fig. 5$(d$–$f)$. As V_0 increases, the $V_1(t)$ oscillations and their spectra evolve in a way that reveals the emergence of chaos through the break down of quasiperiodic motion.

The transition from regular oscillations [Fig. 5(d)], through quasiperiodic [Fig. 5(e)], to chaos [Fig. 5(f)] demonstrates experimentally that a linear resonator can induce chaos in a non-linear system. The resonator imposes a new oscillatory timescale in the system, thus inducing quasiperiodic current oscillations. Under certain conditions, when the nonlinear mixing of oscillations with different time scales is strong enough, the quasiperiodic motion loses its stability [29], which leads to the appearance of chaos in the system (see also [27], Fig. S6).

In conclusion, we have shown both theoretically and

in experiment that a linear resonator can transform the character of the current-time oscillations and, hence, the associated EM radiation, of a microwave generator. In particular, the presence of a *linear* resonator counter-intuitively induces highly nonlinear phenomena including high-frequency chaotic current oscillations. The chaos appears because the external resonator imposes another oscillatory timescale in the active system, thus inducing complex dynamics via the breakdown of the quasiperiodic motion. We believe that the phenomena described here are applicable to other NDC devices, including Gunn diodes [31] and quantum cascade lasers (QCLs) [32, 33]. Note that QCLs are based on weakly-coupled SLs, and are able to generate signals with frequency between 1 THz and the mid infrared range. Herewith, the miniband SLs are promising for generation in sub-THz and lower part of THz range. We suppose that coupling of QCL to a appropriate electrodynamic system can cause the phenomena similar to ones discussed above.

The chaotic high frequency oscillations observed in our experiment may be directly used in a number of modern key technologies [21], that require solid-state fast random number and chaotic signal generators operating at room temperatures. The latter play a crucial role in modern chaos-based communication systems [22, 23], noise radars, and nonlinear antennas [34–39].

This work was partially supported by the President Program (MK–672.2012.2, MD–345.2013.2), RFBR (12-02-33071), EPSRC (EP/F005482/1), and the "Dynasty" Foundation.

[1] F. Brennecke *et al.*, Nature **450**, 268(2007).
[2] A. M. Zagoskin, *Quantum Engineering*, (Cambridge University Press, 2011).
[3] H.-T. Chen *et al.*, Nature **444**, 597 (2006).
[4] C. Walther *et al.*, Science **327**, 1495 (2010).
[5] M. Khajavikhan *et al.*, Nature **482**, 204 (2012).
[6] M. Pöllinger *et al.*, Phys. Rev. Lett. **103**, 053901 (2009).
[7] X.R. Huang *et al.*, Phys. Rev. Lett. **108**, 224801 (2012).
[8] H. Kroemer, Proc. IEEE **52**, 1736 (1964).
[9] J. B. Gunn, IBM J. Res. Develop. **8**, 141 (1964).
[10] H.W. Thim, IEEE Trans. Electron Devices **ED-14** 517 (1967); I.V. Altukhov *et al.*, Sov. Tech. Phys. Lett. **6**, 237 (1980).
[11] L. Esaki and R. Tsu, IBM J. Res. Develop. **14**, 61 (1970).
[12] A. Wacker, Phys. Rep. **357**, 1 (2002).
[13] F. Klappenberger *et al.*, Eur. Phys. J. B **39**, 483 (2004); A. A. Ignatov and V. I. Shashkin, Sov. Phys. JETP **66**, 526 (1987).
[14] T. M. Fromhold *et al.*, Nature **428**, 726 (2004).
[15] N. Alexeeva *et al.*, Phys. Rev. Lett. **109**, 024102 (2012).
[16] M. T. Greenaway *et al.*, Phys. Rev B **80**, 205318 (2009).
[17] K. Hofbeck *et al.*, Phys. Lett. A 218, 349 (1996); H. Eisele *et al.*, Appl. Phys. Lett. **96**, 072101 (2010).
[18] C.P. Endres *et al.*, Rev. Sci. Instrum. **78**, 043106 (2007); P. Khosropanah *et al.*, Opt. Lett. **19**, 2958 (2009); D.G. Paveliev *et al.*, Semicond. **46**, 121 (2012).
[19] K. F. Renk *et al.*, Phys. Rev. Lett. **95**, 126801 (2005); A. A. Ignatov, Semicond. Sci. Technol. **26**, 055015 (2011).
[20] K.A. Lukin *et al.*, Appl. Phys. Lett. **71**, 2484 (1997); ibid 83, 4643 (2003).
[21] Wen Li *et al.*, Phys. Rev. Lett. **111**, 044102 (2013).
[22] Special Issue on Applications of Nonlinear Dynamics to Electronic and Information Engineering (Eited by M. Hasler *et al.*), Proc. IEEE. **90** (5) (2002).
[23] F.C.M. Lau, C. K. Tse. *Chaos-Based Digital Communication Systems: Operating Principles, Analysis Methods, and Performance Evaluation*, (Springer, 2003).
[24] H.-P. Ren *et al.*, Phys. Rev. Lett. **110**, 184101 (2013).
[25] Yu. A. Romanov, Opt. and Spectrosc. **33**, 917 (1972).
[26] Koronovskii A.A. *et al.*, Phys. Rev. B. **88**, (2013) 165304
[27] See Suppl. Mat. at http://link.aps.org/supplemental/... for the Lyapunov analysis, the equivalent circuit of a SL coupled to two resonators, our experimental setup of the SL with external microstrip resonator, the results of our electrodynamic calculations of the mode parameters of the microstrip resonator and illustrations of the transition from periodic to chaotic dynamics in the SL system.
[28] F. Takens, in Lectures Notes in Mathematics, p. 366, (Springer–Verlag, 1981).
[29] V.S. Anishchenko, *Dynamical Chaos - Models and Experiments. Appearance Routes and Structure of Chaos in Simple Dynamical Systems*, (World Scientific, Singapore, 1995).
[30] A. Patanè *et al.*, Appl. Phys. Lett. **81**, 661 (2002).
[31] I.V. Altukhov *et al.*, Sov. Tech. Phys. Lett. **2**, 186 (1976); ibid Sov. Phys. Semicond. **13**, 1148 (1979).
[32] R. Köhler *et al.*, Nature **417**, 156 (2002).
[33] T. Schmielau and M. F. Pereira Jr, Appl. Phys. Lett. **95**, 231111 (2009).
[34] A. A. Koronovskii *et al.* Physics-Uspekhi. **52**, 1213 (2009).
[35] G. S. Nusinovich *et al.*, Phys. Rev. Lett. **87**, 218301 (2001).
[36] V. Dronov *et al.*, Chaos **14**, 30 (2004).
[37] Yu. A. Kalinin *et al.*, Plasma Phys. Rep. **31**, 938 (2005).
[38] B. S. Dmitriev *et al.*, Phys. Rev. Lett. **102**, 074101 (2009).
[39] R. A. Filatov *et al.*, Phys. Plasmas **16**, 033106 (2009).